Exploration of Li–P–S–O composition for solid-state electrolyte materials discovery

Audric Neveu, Vincent Pelé, Christian Jordy, Valérie Pralong

Exploration of Li-P-S-O composition for Solid-State Electrolyte materials discovery

Audric Neveu[1], Vincent Pelé[2], Christian Jordy[2] and Valerie Pralong[1*]

[1]*Normandie Univ, Ensicaen, Unicaen, CNRS, Crismat, 14000 Caen, France*

[2]*SAFT, 111-113 Bd Alfred Daney 33074 Bordeaux, France*

*valerie.pralong@ensicaen.fr

Abstract

A new solid state electrolyte in the system Li-P-S-O is reported with the composition of $Li_{3.2}PS_{3.7}O_{0.3}$. This material is isostructural with $Li_{10}GeP_2S_{12}$, LGPS-type structure. A higher conductivity and lower activation energy than other LPSO materials is reported due to the lattice volume slightly higher. In a full solid-state battery, our material exhibits higher performance than $Li_{10}GeP_2S_{12}$ thank to the formation of an effective SEI. These results indicate that Li-P-S-O system is very promising to find solid electrolyte and should be explored in order to improve the stability of the family of solid state electrolyte at ambient moisture.

Keywords solid state electrolyte, thio-LISICON, LPSO, LGPS, Ionic conductivity

Introduction

Li-ion batteries represent a growing market with the development of electric vehicles. However, the Li-ion technology requires the use of a highly flammable non-aqueous liquid electrolyte that poses safety concerns [1]. Intensive research studies over the past 5 years have focused on the development of all solid state batteries, wherein solid electrolytes are a key components. Solid electrolytes must meet technological requirements such as high ionic conductivity in combination with negligible electronic conductivity, wide voltage window stability (0-5 V), chemical compatibility with cathode and anode materials, relatively simple fabrication at large scale and low cost [2]. Solid lithium conductors can be listed in three groups: inorganic ceramics, organic polymers and composite or hybrid electrolytes being a combination of the first two classes of materials [3]. Within the ceramics electrolytes several oxides with outstanding performances (conductivity in the range of 10^{-4}-10^{-2} S/cm) have been discovered, such as garnets $Li_7La_3Zr_2O_{12}$ [4], perovskites $Li_{3x}La_{2/3-x}TiO_3$ [5], NASICON $(Na,Li)M_2(PO_4)_3$ (M=Ge, Ti, Zr) [6] and LISICON $Li_{14}Zn(GeO_4)_4$ [7]. Argyrodite-type electrolyte Li_6PS_5X (X=Cl, Br, I) [8] and thio-LISICON β–Li_3PS_4 thioposphates have been extensively studied due to their superior ionic conductivity with respect to oxides (~10^{-3} S/cm). For Li_3PS_4, the highest conductivity is obtained for the β-Li_3PS_4 form, stable from 195°C. These phases are promising due to the formation of a stable SEI with lithium displaying good cyclability and long-term compatibility [8]. Large efforts have been dedicated to stabilize β-Li_3PS_4 at room temperature by means of cationic substitution. As an example one can cite $Li_{3.25}[Si_{0.25}P_{0.75}]S_4$ [9] showing a conductivity of 1.22 10^{-3} S/cm at room temperature. Interestingly, Within the exploration of the system Li-(Si/Ge/Sn)-P-S, trying to generate thio-LISICON type structure, Kanno and co-workers [10] reported new thio-phosphates with the general formula $Li_{4-x}Ge_{1-x}P_xS_4$ ($0 < x < 1$) showing a conductivity of 2.2

10^{-3} S/cm at room temperature. Amongst the different solid electrolyte compositions explored in this system (Li-(Ge/Si/Ge/Sn)-P-S), an ionic conductivity comparable to that of liquid electrolytes has been achieved for the composition $Li_{10}GeP_2S_{12}$ (LGPS) reaching a conductivity of 1.2 10^{-2} S/cm at room temperature [11]. LGPS crystallizes in tetragonal space group with a body centered cubic lattice whereas the thio-LISICON family exhibits an orthorhombic structure with hexagonal close pack sulfur sub lattice which is found to be less favorable to the ionic conductivity [12]. The structure of LGPS (Fig. 1, [13]) consists of a 3D network of tetrahedra $(Ge/P)S_4$ and LiS_6 octahedra, which share a common edge and form a 1D chain along the c axis. These chains are connected by tetrahedra PS_4 and $Li4S_4$ by the sharing of a common corner. One-dimensional tunnels along the c-axis are occupied by mobile lithium cations in Li1 and Li3 sites. First principle calculations by Mo et al. [14] predicted the LiS_6 octahedrons were also participating to the conduction along the ab plane (0.9mS/cm), in addition to the lithium ion diffusion along the c axis (40mS/cm), leading to a 3D conductor for this structural family as illustrated by the lithium diffusion (Fig. 1b).

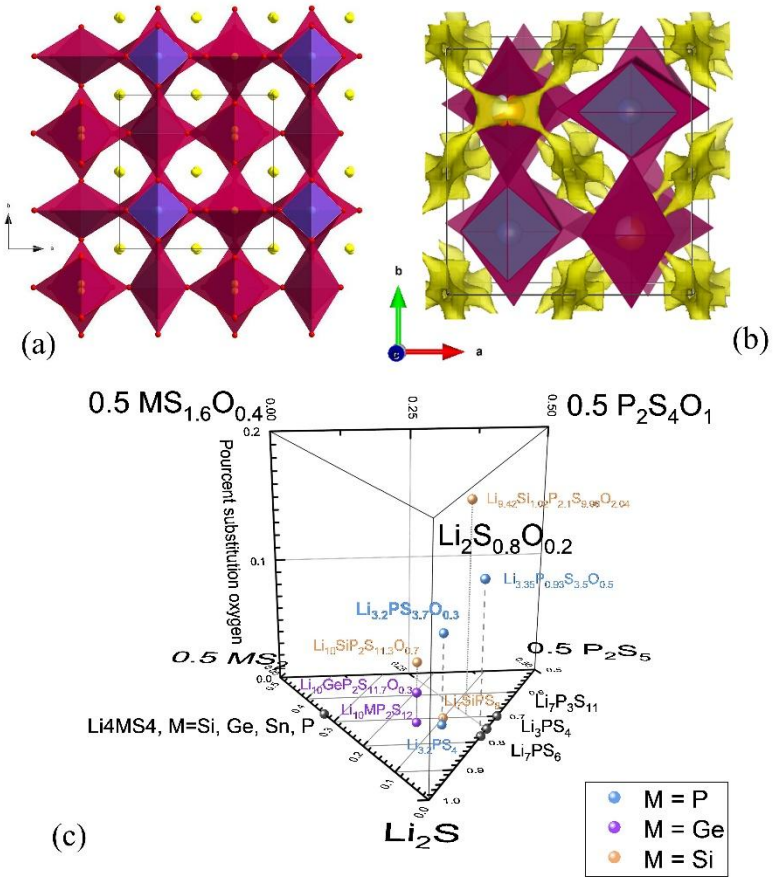

Figure 1: *Projection of $Li_{10}GeP_2S_{12}$ structure showing the 1D tunnel along the c axis occupied by mobile lithium cations (a) and structure with lithium diffusion in yellow calculated by Bond Valence Energy Landscapes BVEL (Bondstr) (b) and phase diagram showing the reported composition with the LGPS-type structure (c).*

In spite of the high conductivity displayed by LGPS, the large concentration of germanium makes this material expensive for widespread applications. Researchers have explored the replacement of germanium by other elements of the IVa group like tin [15], with potential to reduce the raw material cost by a factor of 3 [2], or silicon [16,17]. On Fig. 1c, the main phases showing a LGPS-type structure are reported and we clearly observe the large composition range that could be use. However, LGPS phase has a poor coulombic efficiency

due the degradation of the cathode/Solid Electrolyte Interface (SEI) during charge, which results in the formation of a Li-depleted LGPS layer ultimately leading to capacity fading and increased impedance due to mechanical failure [18]. In addition, LGPS is also instable towards lithium metal anode: Li-Ge alloys, Li_3P and Li_2S were observed by in-situ XPS analysis leading to an increase of the interfacial resistance [19]. In an effort to increase the electrochemical stability window in LGPS, Sun et al. [20] investigated the partial substitution of sulfur by oxygen in $Li_{10}GeP_2S_{12-x}O_x$ (LGPSO) with $0<x<0.9$, which result in an increase of the coulombic efficiency. Following this idea of oxygen-sulfur substitution together with the aim to reduce the amount of germanium, Kanno et al. [20,21] have discovered a new family of solid electrolytes based also on Thio-phosphate in the system Li_2S-P_2S_5-P_2O_5, showing the LGPS type structure, $Li_{3+5x}P_{1-x}S_{4-z}O_z$ (LPSO) with x = 0.03–0.08, z =0.4–0.8. Despite a lower ionic conductivity, LGPSO and LPSO solid electrolytes are showing a better stability when cycled in half-cells due to the partial substitution of S for O in LPSO. The SEI formed during the cycling of these compounds is more efficient and allows a much better coulombic efficiency [22].

Interestingly, A new stable composition was also discovered by Kanno group [23] in the system Li-P-S with the composition $Li_{9.6}P_3S_{12}$ (*i.e.* $Li_{3.2}PS_4$). For such a composition, a mix valence is required and the phosphorous oxidation state is expected to be +4.8. This phase crystallizes also with the LGPS type structure and shows a good conductivity of 1.19 10^{-3} S/cm at room temperature associated with a good stability toward lithium metal with minimum irreversible capacity [25]. Note that this phase seems to be difficult to prepare with a high purity and was previously reported with 35 wt% of β-Li_3PS_4 as a secondary phase.

In this work, we report the synthesis and electrochemical characterizations of $Li_{3.2}P^{+4.8}S_{3.7}O_{0.3}$. Indeed, based on the literature report, we believe that a partial substitution of

S for O in $Li_{3.2}PS_4$ will also lead to LGPS type structure with enhanced chemical stability properties and make also this phase easier to be prepared.

Experimental techniques

For the synthesis, we use classical mechanochemical synthesis followed by annealing at 200°C in sealed tubes under vacuum [17,25,26]. Li_2S (Alfa Aesar 99.9%), P_2S_5 (Aldrich 99%), P_2O_5 (Alfa Aesar 99.99%), GeS_2 (home made with stoichiometric amount of Ge° and S in sealed tube at 500°C) and red phosphorus (Aldrich 99,99%) were used and all the chemicals were handled under a high purity argon atmosphere (H_2O<0.1 ppm, O_2<0.1ppm). Regarding the source for the oxygen, we have tried different precursor such as Li_3PO_4, Li_2O or P_2O_5. Interestingly, the synthesis was successful only starting from P_2O_5 as precursor. Note therefore that we choose the oxygen concentration of 0.3 which corresponds to 7,5% of oxygen substitution. Such value is in the range of other substitution amount reported in the literature (between 2,5 and 17%). The precursors were weighed in stoichiometric ratios and ground by planetary milling for 35h at 500 RPM (Fritsh, 25 ml ZrO_2 bowls with 4 balls). Bowls are scraped every 5 hours in order to peel off the powder from the walls. The mixture is then pelletized at 160 MPa, placed in a sealed tube with a carbon coating and then heated at 200°C for 4h for $Li_{3.2}PS_{3.7}O_{0.3}$ compounds and at 500°C for 4 hours to prepare the phase $Li_{10}GeP_2S_{12}$.

$Li_{3.2}PS_{3.7}O_{0.3}$ was measured in capillary (radius = 0.25 mm, thickness = 0.01 mm) with a Philips X'Pert diffractometer with Bragg-Brentano geometry ($CuK_{\alpha 1,2}$ radiation). Rietveld Refinement of the patterns was carried out using the Rietveld method in Fullprof suite software. Temperature X-ray diffraction analysis was carried out between 30 and 300°C using a Philips X'Pert diffractometer with Bragg-Brentano geometry (Co radiation). The specimen

was put under vacuum and heated with a rate 1°C/min in chamber temperature. Diffraction data were collected from 10° to 50.0° in 2θ.

The thermal properties of the $Li_{3.2}PS_{3.7}O_{0.3}$ were investigated by combined Differential scanning calorimetry (DSC) and Thermogravimetric analysis (TGA) with a Netzsch STA 449F3. Sample was put under argon in alumina crucible and heated with a rate 1°C/min.

For impedance spectroscopy measurement, samples were pelletized (diameter = 10 mm, thickness ≈ 0.1 cm) under 160 MPa and gold plated. The sample is then placed in the Bio-logic Controlled Environment Sample Holder (CESH). A signal with an amplitude of 50 mV and frequencies between 1 MHz and to 0.1 Hz was applied using a frequency response analyzer (Solartron, 1260). Temperature was controlled by the Bio-logics Intermediate Temperature System (ITS) between 80°C and -40°C.

For symmetric cell, 50mg of $Li_{3.2}PS_{3.7}O_{0.3}$ was pressed at 255 MPa in the cell presented previously [24]. Li metal was then added on each side of the electrolyte and pressed with the screws of the cells. Note therefore that we only cycle at 0.1mA/cm^2 this type of cell. For cycling voltammetry, 50mg of $Li_{3.2}PS_{3.7}O_{0.3}$ was pressed at 255 MPa. Platine electrode was added on one side of the electrolyte and pressed at 255MPa. Lithium metal was added on the other side of the electrolyte and pressed with screws of the cells. For full cells, two mixtures are prepared. A mixture of 70w% of pure $LiNi_xCo_yAl_zO_2$ (NCA) without any coating and 30w% of electrolyte, which forms the positive electrode, and a mixture with 66w% of graphite (MGPT16) and 33w% of electrolyte, which forms the negative electrode. For assembling, About 40 mg of an electrolyte was pressed at 255MPa and then negative and positive electrodes (about 15mg for each) were pressed on each side of the electrolyte at 255MPa. The calculated loading was about 38 mg/cm² (surface of the cell is 0.28cm²). The pressure is maintained by the screws of the cell. Half-cell were made with the same protocol:

about 40mg of $Li_{3.2}PS_{3.7}O_{0.3}$ was pressed at 255 MPa and a mix of NCA/electrolyte was pressed on one side of the electrolyte at 255MPa. The lithium was finally added on the other side of the electrolyte and pressed with screws of the cells

The amount of H_2S generated from the lithium solid electrolyte exposed at ambient was measured with a H_2S sensor (Croncow, Gasman). About 30±2 mg of powder was placed in 4000 cm^2 desiccator. In order to insure a constant humidity level, 20mL of H_2O are placed in the desiccator. The H_2S (in mg/m^3) generated was calculated from the H_2S concentration measured by the H_2S sensor in ppm. For the conversion, we use $1mg/m^3 = (22.4/M_{H2S}) = 0.67ppm$. Note that 7 mg/m^3 is the exposure limit value for the French standards from the National Research and Security Institute.

Results and discussion

The XRD pattern of the phase $Li_{3.2}PS_{3.7}O_{0.3}$ is reported on Figure 2. The material could be indexed with space group ($P4_2/nmc$) and lattice parameters similar to those of other LGPS-type compounds [11,23,27]. Despite our synthesis optimization, 5.23wt% of Li_2S is still present as impurity. Our material is air sensitive therefore chemical analysis are difficult to do and in order to properly confirm the exact composition of this phase, a combined neutron-synchrotron analysis needs to be performed. Nevertheless, taking into account the 5% of Li_2S impurity, one could hypothesis that the composition will be close to '$Li_3P^{+4.8}S_{3,6}\square_{0,1}O_{0,3}$'. The structural model reported for the phase $Li_{3.2}PS_4$ were used as initial parameters for the Rietveld refinement [23]. Atomic positions and the occupancy of lithium were fixed. Smaller lattice parameters are observed for $Li_{3.2}PS_{3.7}O_{0.3}$ compare to $Li_{10}GeP_2S_{12}$ [11] and $Li_{3.2}PS_4$ [23], (Table 1). A similar effect has been observed with other LPSO compound that was explained by the difference of the substituted element [27]. Germanium has an ionic

radius of 0.39 Å while phosphorus has an ionic radius of 0.17 Å. Likewise with oxygen, which is smaller than sulfur (1.34 Å for 1.84 Å). As we substituted less sulfur than $Li_{3.35}P_{0.93}S_{3.5}O_{0.5}$, higher lattice parameters are observed for $Li_{3.2}PS_{3.7}O_{0.3}$.

	a (Å)	c (Å)	V (Å3)	Conductivity (S/cm)	Activation energy (kJ/mol)
$Li_{10}GeP_2S_{12}$ LGPS [11]	8.71771(5)	12,63452(10)	960.20	12 10^{-3} (25°C)	24.0 (25 eV)
$Li_{3.2}PS_4$ [23]	8.7144(4)	12.4677(7)	946.80	1.19 10^{-3} (27°C)	28.0 (0.29 eV)
$Li_{3.35}P_{0.93}S_{3.5}O_{0.5}$ [27]	8.3702(3)	12.3023(6)	861.92(6)	8.76 10^{-5} (27°C)	36.6 (0.38 eV)
$Li_{3.2}PS_{3.7}O_{0.3}$ [this work]	8.591(1)	12.315(1)	908.912(1)	1.19 10^{-4} (25°C)	33.9 (0.35 eV)

Table 1. Lattice parameter, volume cell, conductivity and activation energy of $Li_{3.2}PS_{3.7}O_{0.3}$ and different compounds from literature.

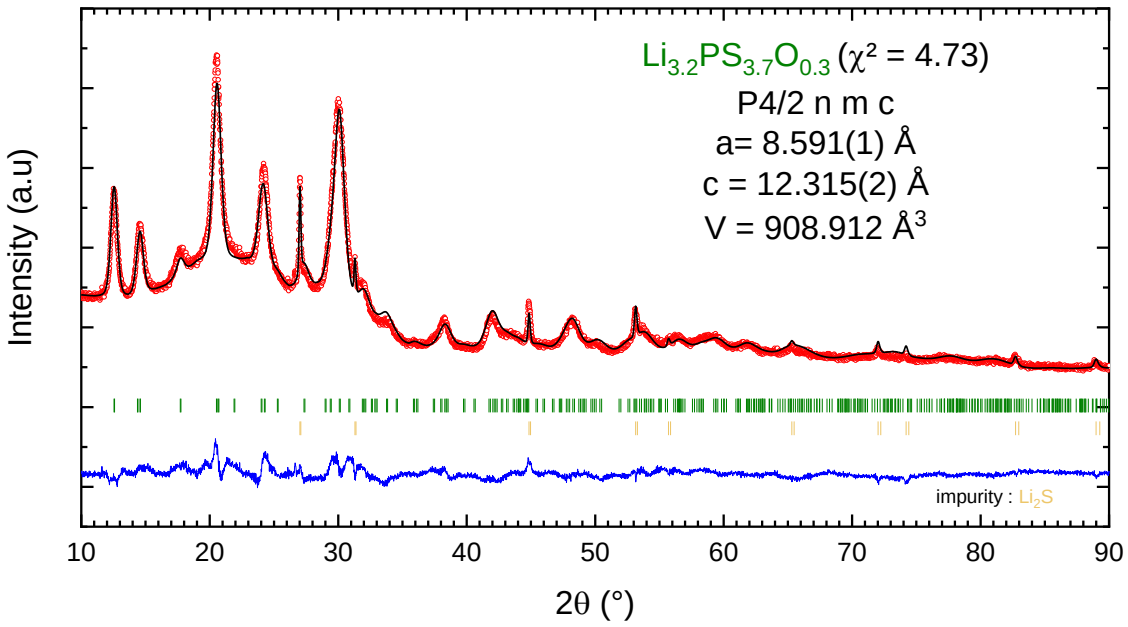

Figure 2. Rietveld refinements of XRD pattern of $Li_{3.2}PS_{3.7}O_{0.3}$.

We test the thermal stability of our compound under argon by means of coupled DSC-TGA and also thermodiffraction (Fig. 3a). The phase $Li_{3.2}PS_{3.7}O_{0.3}$ is stable in the temperature range of 30-300°C under vacuum. Indeed, no change could be observed on the thermodiffraction. Only 2Wt% of mass change is observed between 25°C and 150°C on TGA, associated with a small variation on the DCS response and could be ascribe to a surface reaction (Fig. 3b). No phase crystallization is observed, suggesting that there was no amorphous phase in the composite.

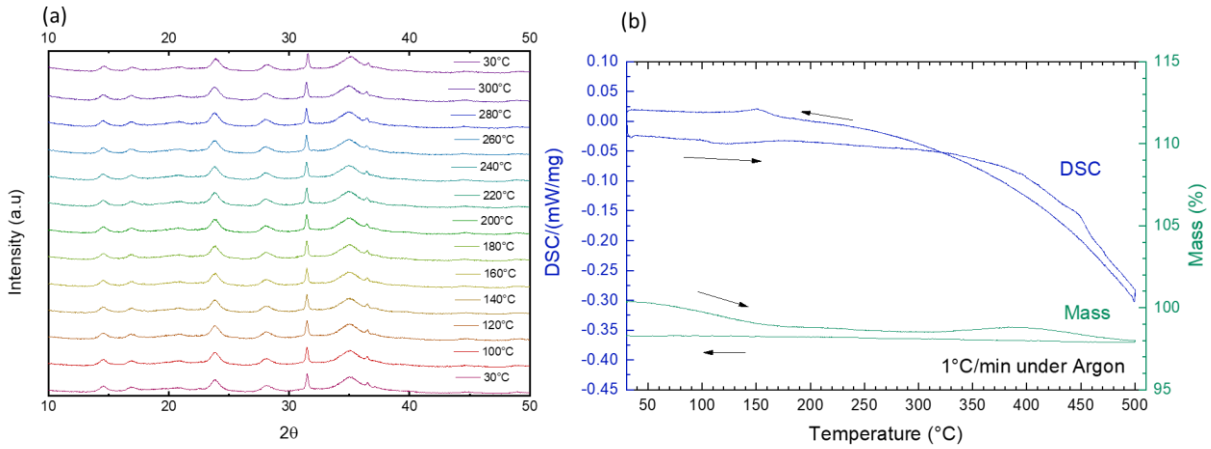

Figure 3. Thermodiffraction of $Li_{3.2}PS_{3.7}O_{0.3}$ under vacuum (a) and DSC-TGA plot under argon at 1°/min (b).

The ionic conductivity has been studied by AC impedance spectroscopy. The Nyquist diagram of $Li_{3.2}PS_{3.7}O_{0.3}$ and the equivalent circuit used for calculation are shown in Figure 4 a,b. Two half circle following with a spick are visible. Ec-Lab sofware are used for the fit. The impedance response consists of a succession of resistance and a constant-phase element (CPE) in parallel, with all being in series with a CPE. The capacity of the CPE can be estimate with the Brug formula [28]:

$$\frac{1}{2\pi(RQ_o)^{\frac{1}{\alpha}}} = \frac{1}{2\pi RC}$$

With Q_0 and α the CPE parameters. The capacity calculated for the first and second cycle is about 10^{-12} F and 10^{-9} F respectively. Following this values, the first cycle can be attribute to the bulk conductivity and the second to the grain boundary conductivity [29]. The total conductivity is obtain by summing the value of the two resistance. These conductivities are reported in an Arrhenius diagram with others compounds from literature (Fig. 4c). The total conductivity of our compound is 1.19 10^{-4} S/cm at 25°C (Table 1). This value is one order lower than $Li_{3.2}PS_4$, consistent with the smaller lattice volume [23]. However, this ionic conductivity is higher than other LPSO as the lattice volume is higher [27].

The activation energies were calculated from linear extrapolation of the Arrhenius plot. The values obtained for $Li_{3.2}PS_{3.7}O_{0.3}$ was 33.9 kJ/mol (0.35 eV). This value is larger than $Li_{3.2}PS_4$ but lower than $Li_{3.35}P_{0.93}S_{3.5}O_{0.5}$ meaning that stronger electrostatic attraction between O atoms and Li ions have a function in conduction mechanism.

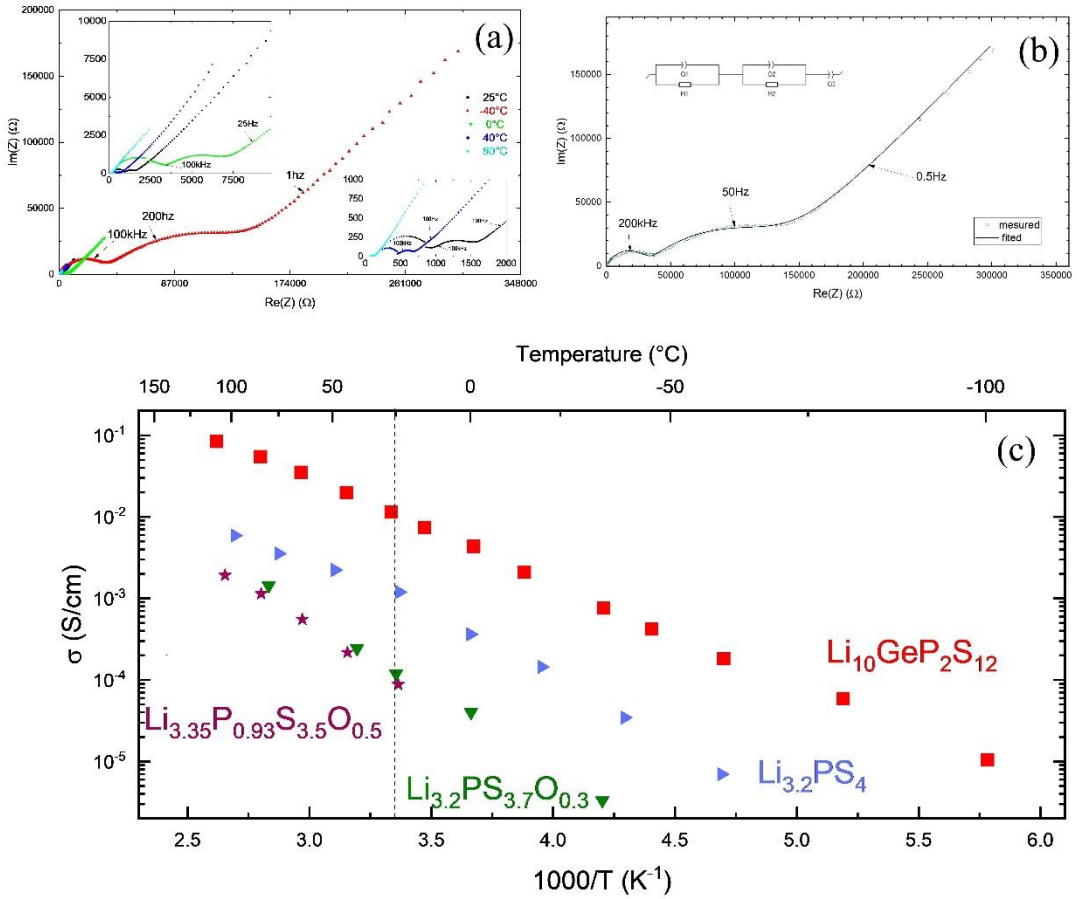

Figure 4. Nyquist impedance plots for $Li_{3.2}PS_{3.7}O_{0.3}$ from -40°C to 80°C (a) and at -40°C with the equivalent circuit used for the fit (b). Arrhenius plot of $Li_{3.2}PS_{3.7}O_{0.3}$ and compounds from literature (c).

The ionic conductivity and activation of energy of the best-reported thio-LISICON solid electrolytes are compared in Table 1. Even if the pure LGPS shows better conductivity than LPSO type phases with a conductivity one order of magnitude higher, due to the reaction between Ge and lithium reported in literature [30], we expect a better electrochemical stability of our material. Then, a symmetric Li/$Li_{3.2}PS_{3.7}O_{0.3}$/Li cell was configured to demonstrate the cyclability and long-term compatibility of this composition with metallic lithium. The flat voltage–time profiles of the solid electrolyte symmetric cells are shown in Figure 5 at a current of 0.1 mA/cm^2. They exhibit a good cycling stability of discharge and charge and

good compatibility between solid electrolytes and lithium metal compare to the cell with LGPS. The overpotential of our material during cycling remains stable around at 25 mV after 25 cycles whereas the overpotential of Li/LGPS/Li reach 50 mV. Note that in addition to the large polarization increase upon cycling for the Li/LGPS/Li cell, one observe for each current step, a potential decrease versus time. Such behavior characterize a poor conductivity at the interfaces, suggesting an insulating SEI formation. The resultant dc Li ionic conductivity (σ_{dc}) can be derived from the polarization voltage divided by the applied current. Thus, we found a σ_{dc} of 2.2 10^{-4} S/cm. This value is consistent with the one obtained from the Nyquist plot from EIS measurement (σ_{ac}= 1.19 10^{-4}S/cm). When comparing with the cycling behavior of the symmetric cell with LGPS, it is clear that our material is compatible with metallic lithium electrode.

For the CV measurement (Fig. 5b), we use a potential window -0.2 – 5 V vs Li^+/Li with a scan rate of 10mV/s in a Li/$Li_{3.2}PS_{3.7}O_{0.3}$/Pt cell. No significant redox peaks (expecting the one at 0.0V) are observed in the potential window of 0 to 5V vs Li^+/Li, showing then the excellent electrochemical stability of this material that could be used in a wide voltage range. Note that the small current observed between 0.25 and 1.25V could be due to the low ionic conductivity of this material.

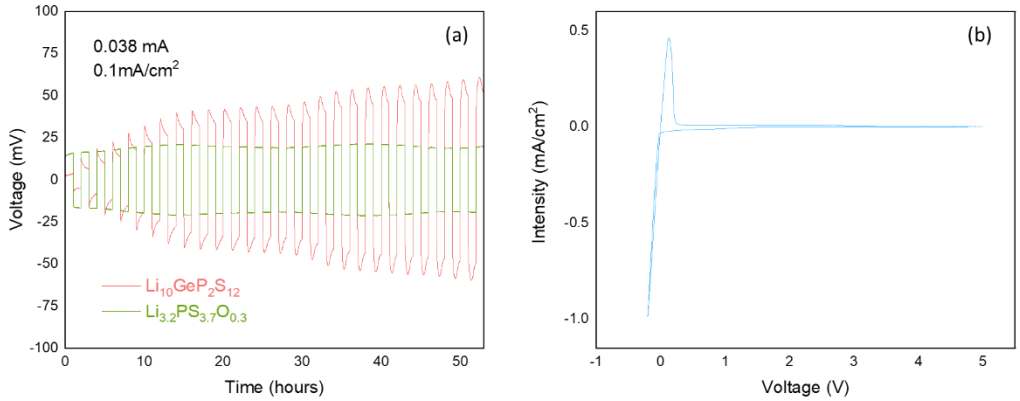

Figure 5. Lithium cyclability in the symmetric Li/ $Li_{3.2}PS_{3.7}O_{0.3}$/Li and Li/LGPS/Li cells under a current density of 0.1mA/cm^2 at room temperature (a) and Cycling voltammetry of a Li/$Li_{3.2}PS_{3.7}O_{0.3}$/Pt cell at 10 mV/s (b).

As our material showed good result with symmetric cell and CV measurement, we tested it as solid electrolyte in half all-solid-state batteries. Half-cell were assembled with $LiNi_{1/3}Co_{1/3}Al_{1/3}O_2$ (NCA) as active material. The positive electrode is a mixture of NCA and $Li_{3.2}PS_{3.7}O_{0.3}$ at a weight ratio of 7:3 in order to ensure a good ionic conductivity between different solid element [31]. The first 5 cycles of this cell at a rate of C/40 are represented on Figure 6a. The first charge gives a capacity of 166 mAh/g and an irreversible of 56 mAh/g is observed during the the first discharge. This irreversible implying some Li was consumed in the 1st cycle probably by interfacial reactions [23,31]. The other charge-discharge showed a good reversibility of about 100mAh/g. The small change between each cycle can by explained by our cell that is not designed for lithium metal which is a very soft metal.

Then, we test $Li_{3.2}PS_{3.7}O_{0.3}$ as solid electrolyte in full all-solid-state batteries. Full cells were assembled with the same active material as half-cell (NCA) and graphite as negative material. The same mixture as the half-cell is used for active material and mixture of graphite and $Li_{3.2}PS_{3.7}O_{0.3}$ at a weight ratio of 66:33 is used as negative material. Figure 6b shows 10 charges and discharges curves of the solid-state full-cell battery at a rate of 0.05 C (I=0.038mA/cm^2) made with $Li_{3.2}PS_{3.7}O_{0.3}$ material. The first charge achieves a capacity of 180 mAh/g. However, as we observed with half-cell, a large irreversible capacity were observed at the first cycle (50mAh/g), implying some Li was consumed in the 1st cycle probably by interfacial reactions [23,31]. The performance of $Li_{3.2}PS_{3.7}O_{0.3}$ have been compared with $Li_{10}GeP_2S_{12}$ (Fig. 6c,d). $Li_{10}GeP_2S_{12}$ showed a coulombic efficiency of 18% in

the first cycle. As the literature already shown, the lowest performance of $Li_{10}GeP_2S_{12}$ comes to a none-effective SEI formation [19,22,31]. A more effective SEI was formed with $Li_{3.2}PS_{3.7}O_{0.3}$ as a better coulombic efficiency is observed (71%). These interface result in better performance. For $Li_{3.2}PS_{3.7}O_{0.3,}$ the first discharge has a capacity of 128 mAh/g and the 10^{th} keep a capacity of 110 mAh/g where $Li_{10}GeP_2S_{12}$ reports at the first discharge a capacity of 29.7 mAh/g and fading to 12.7 mAh/g for the 10^{th} discharge. Kanno demonstrated the same trend for LGPS in his paper [20].

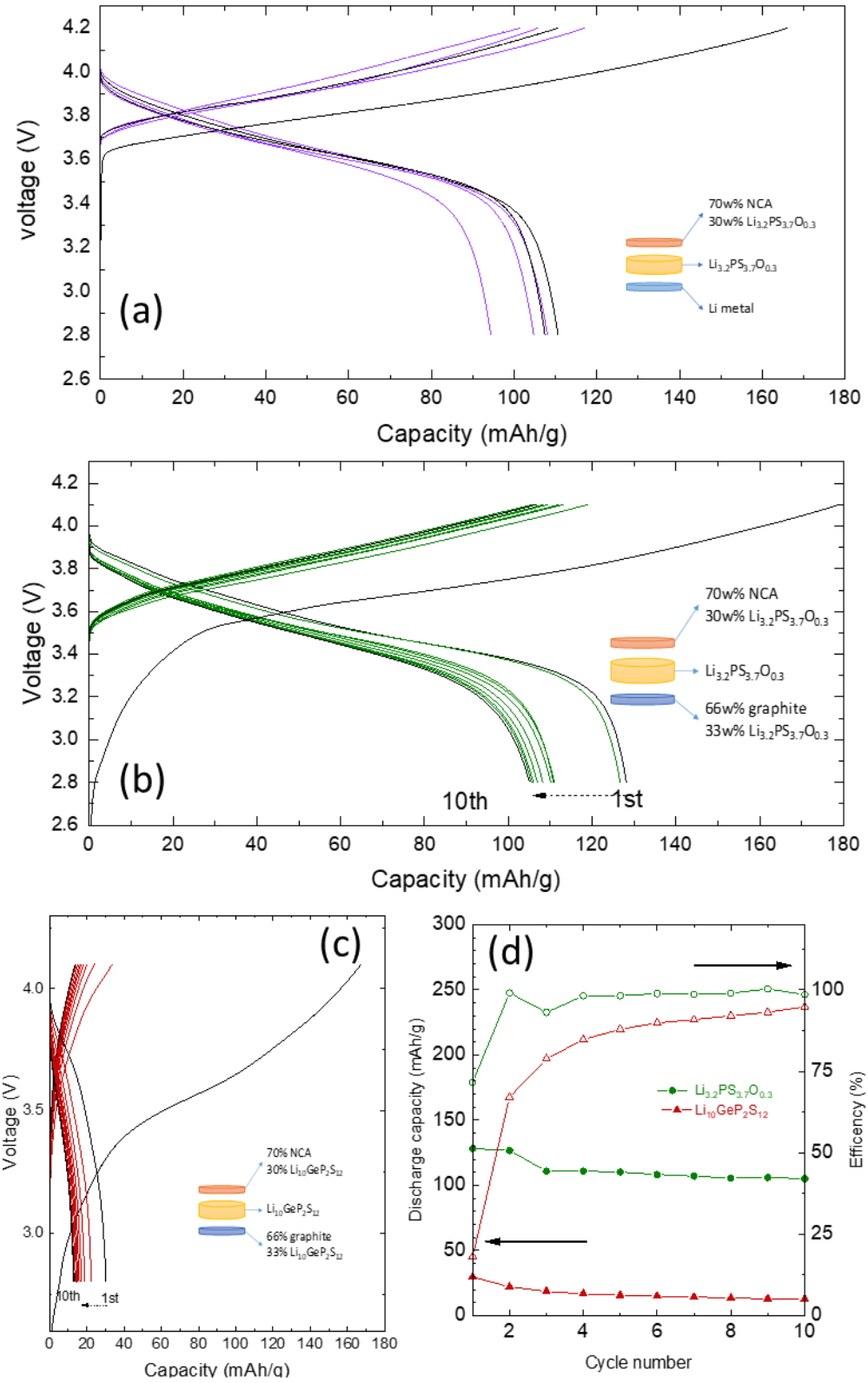

Figure 6: Charge-discharge profiles of half cells NCA:$Li_{3.2}PS_{3.7}O_{0.3}$/$Li_{3.2}PS_{3.7}O_{0.3}$/Li° at a rate of C/40 (a) Charge-discharge profiles of full cells NCA:$Li_{3.2}PS_{3.7}O_{0.3}$/$Li_{3.2}PS_{3.7}O_{0.3}$/$Li_{3.2}PS_{3.7}O_{0.3}$:MGPT16 at rate of C/20 (b) Charge-discharge

profiles of full cells NCA:LGPS/LGPS/LGPS:MGPT16 at rate of C/20 (c) and Cycling characteristics for discharge capacity and efficiency for all-solid-state cells made with $Li_{3.2}PS_{3.7}O_{0.3}$ *and* $Li_{10}GeP_2S_{12}$ *(d).*

In order to evaluate the stability in ambient environment, these compounds were exposed to humidity of the ambient atmosphere. Figure 7 shows the H_2S amount generated from LPSO compound, Li_2S and $Li_{10}GeP_2S_{12}$. The new synthetized compound shows a weak stability at ambient moisture, which is due to the 5wt% of Li_2S impurity. The gas released after 30 min for $Li_{3.2}PS_{3.7}O_{0.3}$ is 25 mg/m^3. This value is more than 2.5 times the amount of gas released for $Li_{10}GeP_2S_{12}$ (10 mg/m^3) but consistent with the value that is expected with a material containing 5% amount of Li_2S as impurity.

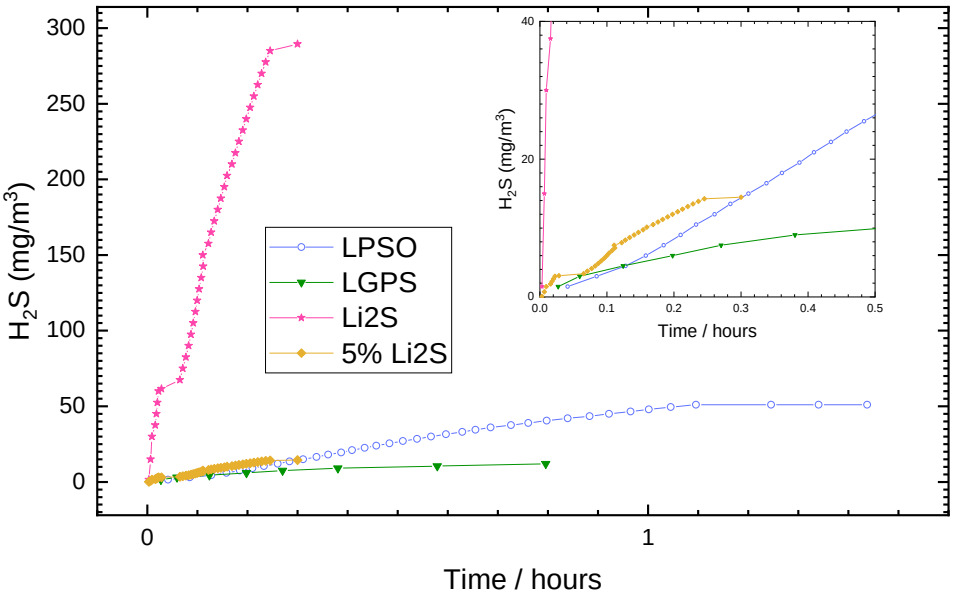

Figure 7. H_2S amount generated from $Li_{3.2}PS_{3.7}O_{0.3}$, Li_2S and $Li_{10}GeP_2S_{12}$ compound after exposition to air.

Conclusions

New compound from LPSO family was synthetized by typical ball milling–annealing synthesis. The structure of $Li_{3.2}PS_{3.7}O_{0.3}$ is isostructural with $Li_{10}GeP_2S_{12}$ with smaller lattice volume. This compound exhibit a higher conductivity and lower activation energy than other LPSO material, as the lattice volume was slightly higher than other LPSO. In a full solid-state battery, synthetized LPSO exhibits higher performance than $Li_{10}GeP_2S_{12}$ thank to the formation of an effective SEI. A combined neutron diffraction and X-ray synchrotron study will be necessary to refine the structure and access to the chemical composition with accuracy. These results indicate that Li-P-S-O system is very promising as solid electrolyte and should be explored in order to improve the stability of the family of solid-state electrolyte at ambient moisture.

Acknowledgement

The authors thank J. Jean, S. Gascoin for technical help and M. Diaz-Lopez for scientific discussions. We gratefully acknowledge the CNRS, the Minister of Education and Research, Normandy region and SAFT through the contract SAFT-CNRS n°2019-42356.

References

[1] X. Wu, K. Song, X. Zhang, N. Hu, L. Li, W. Li, L. Zhang, and H. Zhang, Front. Energy Res. **7**, (2019).

[2] A. Manthiram, X. Yu, and S. Wang, Nat. Rev. Mater. **2**, (2017).

[3] F. Zheng, M. Kotobuki, S. Song, M. O. Lai, and L. Lu, J. Power Sources **389**, 198 (2018).

[4] R. Murugan, V. Thangadurai, and W. Weppner, Angew. Chem. Int. Ed. **46**, 7778 (2007).

[5] Y. Inaguma, C. Liquan, M. Itoh, T. Nakamura, T. Uchida, H. Ikuta, and M. Wakihara, Solid State Commun. **86**, 689 (1993).

[6] J. B. Goodenough, H. Y. P. Hong, and J. A. Kafalas, Mater. Res. Bull. **11**, 203 (1976).

[7] H. Y.-P. Hong, Mater. Res. Bull. **13**, 117 (1978).

[8] Z. Liu, W. Fu, E. A. Payzant, X. Yu, Z. Wu, N. J. Dudney, J. Kiggans, K. Hong, A. J. Rondinone, and C. Liang, J. Am. Chem. Soc. **135**, 975 (2013).

[9] L. Zhou, A. Assoud, A. Shyamsunder, A. Huq, Q. Zhang, P. Hartmann, J. Kulisch, and L. F. Nazar, Chem. Mater. **31**, 7801 (2019).

[10] R. Kanno and M. Murayama, J. Electrochem. Soc. **148**, A742 (2001).

[11] N. Kamaya, K. Homma, Y. Yamakawa, M. Hirayama, R. Kanno, M. Yonemura, T. Kamiyama, Y. Kato, S. Hama, K. Kawamoto, and A. Mitsui, Nat. Mater. **10**, 682 (2011).

[12] Y. Wang, W. D. Richards, S. P. Ong, L. J. Miara, J. C. Kim, Y. Mo, and G. Ceder, Nat. Mater. **14**, 1026 (2015).

[13] O. Kwon, M. Hirayama, K. Suzuki, Y. Kato, T. Saito, M. Yonemura, T. Kamiyama, and R. Kanno, J. Mater. Chem. A **3**, 438 (2014).

[14] Y. Mo, S. P. Ong, and G. Ceder, Chem. Mater. **24**, 15 (2012).

[15] P. Bron, S. Johansson, K. Zick, J. Schmedt auf der Günne, S. Dehnen, and B. Roling, J. Am. Chem. Soc. **135**, 15694 (2013).

[16] S. Hori, K. Suzuki, M. Hirayama, Y. Kato, T. Saito, M. Yonemura, and R. Kanno, Faraday Discuss. **176**, 83 (2015).

[17] Y. Sun, K. Suzuki, S. Hori, M. Hirayama, and R. Kanno, Chem. Mater. **29**, 5858 (2017).

[18] W. Zhang, F. H. Richter, S. P. Culver, T. Leichtweiss, J. G. Lozano, C. Dietrich, P. G. Bruce, W. G. Zeier, and J. Janek, ACS Appl. Mater. Interfaces **10**, 22226 (2018).

[19] S. Wenzel, S. Randau, T. Leichtweiß, D. A. Weber, J. Sann, W. G. Zeier, and J. Janek, Chem. Mater. **28**, 2400 (2016).

[20] Y. Sun, K. Suzuki, K. Hara, S. Hori, T. Yano, M. Hara, M. Hirayama, and R. Kanno, J. Power Sources **324**, 798 (2016).

[21] S. Hori, K. Suzuki, M. Hirayama, Y. Kato, and R. Kanno, Front. Energy Res. **4**, (2016).

[22] M. Sakuma, K. Suzuki, M. Hirayama, and R. Kanno, Solid State Ion. **285**, 101 (2016).

[23] Y. Kato, S. Hori, T. Saito, K. Suzuki, M. Hirayama, A. Mitsui, M. Yonemura, H. Iba, and R. Kanno, Nat. Energy **1**, 16030 (2016).

[24] X. Wu, M. El Kazzi, and C. Villevieille, J. Electroceramics **38**, 207 (2017).

[25] Y. Kato, R. Saito, M. Sakano, A. Mitsui, M. Hirayama, and R. Kanno, J. Power Sources **271**, 60 (2014).

[26] K.-H. Kim and S. W. Martin, Chem. Mater. **31**, 3984 (2019).

[27] K. Suzuki, M. Sakuma, S. Hori, T. Nakazawa, M. Nagao, M. Yonemura, M. Hirayama, and R. Kanno, Solid State Ion. **288**, 229 (2016).

[28] G. J. Brug, 21 (n.d.).

[29] J. T. S. Irvine, D. C. Sinclair, and A. R. West, Adv. Mater. **2**, 132 (1990).

[30] C. Wang, K. R. Adair, J. Liang, X. Li, Y. Sun, X. Li, J. Wang, Q. Sun, F. Zhao, X. Lin, R. Li, H. Huang, L. Zhang, R. Yang, S. Lu, and X. Sun, Adv. Funct. Mater. **29**, 1900392 (2019).

[31] W. Zhang, D. A. Weber, H. Weigand, T. Arlt, I. Manke, D. Schröder, R. Koerver, T. Leichtweiss, P. Hartmann, W. G. Zeier, and J. Janek, ACS Appl. Mater. Interfaces **9**, 17835 (2017).